ACCOUNTS of chemical research

Article

Cite This: Acc. Chem. Res. 2019, 52, 2647−2656

pubs.acs.org/accounts

Deactivation of Zeolites and Zeotypes in Methanol-to-Hydrocarbons Catalysis: Mechanisms and Circumvention

Andrew Hwang*,†,‡ and Aditya Bhan*,†

†Department of Chemical Engineering and Materials Science, University of Minnesota, Minneapolis, Minnesota 55455, United States

CONSPECTUS: Solid catalysts deployed in industrial processes often undergo deactivation, requiring frequent replacement or regeneration to recover the loss in activity. Regeneration occurs under conditions distinct from, and typically more harsh than, the catalysis, placing strict requirements on physicochemical material properties that divert catalyst optimization toward addressing regenerability over high activity and selectivity. Deactivation arises from mechanical, structural, or chemical modifications to active sites, promoters, and their surrounding matrices, and the prevailing mechanism for deactivation varies with the reaction, the catalyst, and the reaction conditions. Methanol-to-hydrocarbons processes utilize zeolites and zeotypes—crystalline, microporous oxides widely deployed as catalysts in the refining and petrochemical industries—as solid acid catalysts. Deposition and growth of highly unsaturated carbonaceous residues within the micropores congest molecular transport and block active sites, resulting in deactivation. In this Account, we describe studies probing the underlying mechanisms of deactivation in methanol-to-hydrocarbons catalysis and discuss examples of leveraging the acquired mechanistic insights to mitigate deactivation and prolong catalyst lifetime. These fundamental principles governing carbon deposition within zeolites and zeotypes provide opportunity to broaden versatility of processes for C_1 valorization and to relax constraints imposed by hydrothermal catalyst stability considerations to achieve more active and more selective catalysis.

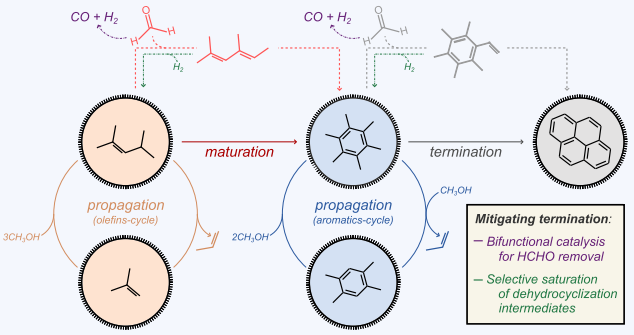

Methanol-to-hydrocarbons catalysis occurs via a chain carrier mechanism. A zeolite/zeotype cavity hosts an unsaturated hydrocarbon guest to together constitute the supramolecular chain carrier that engages in a complex network of reactions for chain carrier propagation. Productive propagation reactions include olefin methylation, aromatic methylation, and aromatic dealkylation. Methanol undergoes unproductive dehydrogenation to formaldehyde via methanol disproportionation and olefin transfer hydrogenation. Subsequent alkylation reactions between formaldehyde and active olefinic/aromatic cocatalysts instigate cascades for dehydrocyclization, resulting in the formation of inactive polycyclic aromatic hydrocarbons and termination of the chain carrier.

Addition of a distinct catalytic function that selectively decomposes formaldehyde mitigates chain carrier termination without disrupting the high selectivity to ethylene and propylene in methanol-to-hydrocarbons catalysis on small-pore zeolites and zeotypes. The efficacy of this bifunctional strategy to prolong catalyst lifetime increases with increasing proximity between the active sites for formaldehyde decomposition and the H^+ sites of the zeolite/zeotype. Coprocessing sacrifical hydrogen donors mitigates chain carrier termination by intercepting, via saturation, intermediates along dehydrocyclization cascades. This strategy increases in efficacy with increasing concentration of the hydrogen donor and provides opportunity to realize steady-state methanol-to-hydrocarbons catalysis on small-pore zeolites and zeotypes.

INTRODUCTION

Methanol-to-hydrocarbons catalysis provides a route to upgrade fungible, abundant, and renewable carbonaceous feedstocks into petrochemical precursors and transportation fuels.[1] The catalysis utilizes zeolites and zeotypes—crystalline microporous oxides with pores of molecular dimension (ca. 1 nm)—as solid acids.[2,3] Many commercial plants today deploy this catalysis for valorization of coal to ethylene and propylene.[4−6] The technology can in principle be extended to include nonfossil feedstocks amenable to syngas production[1,7−9] and to produce other valuable hydrocarbon products by exploiting the diverse shape selectivity afforded by the catalogue of zeolite/zeotype structures.[10]

The catalysis proceeds via a chain carrier mechanism[11] with distinct initiation, propagation, and termination phases (Scheme 1). Initiation events[12−22] result in the formation of unsaturated hydrocarbons within the micropores of the solid acid. The hydrocarbon guest and zeolite/zeotype host together form the hybrid organic−inorganic chain carrier that engages in H^+-catalyzed reactions for C−C bond formation and C−C

Received: April 22, 2019
Published: August 12, 2019

DOI: 10.1021/acs.accounts.9b00204
Acc. Chem. Res. 2019, 52, 2647−2656

Scheme 1. Chain Carrier Mechanism for Methanol-to-Hydrocarbons Catalysis on Zeolites/Zeotypes with Initiation, Propagation, and Termination Phases

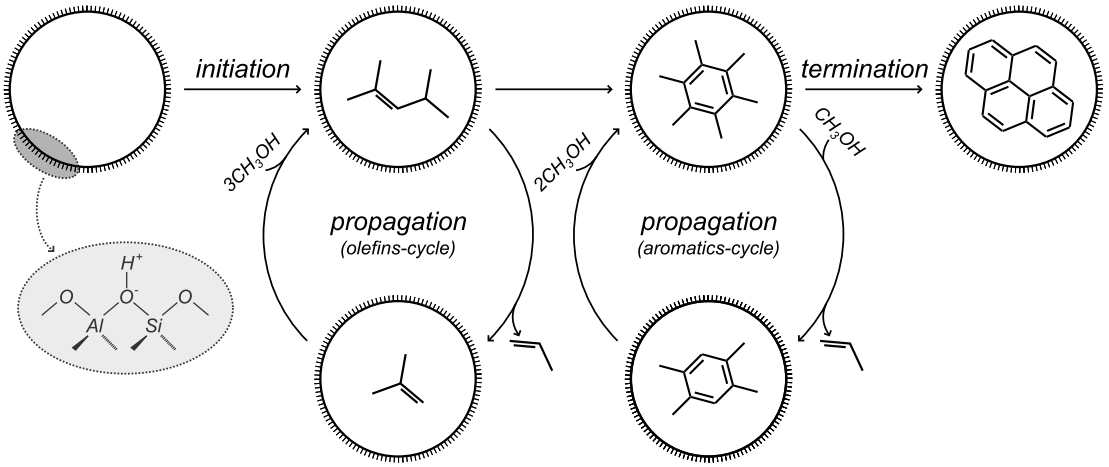

bond scission during chain carrier propagation. Olefins and aromatics constitute the organic component, the so-called "hydrocarbon pool",[23−25] and a "dual-cycle" scheme[26] summarizes the complex network of propagation reactions.[26,27] Olefins undergo methylation and cracking in the *olefins cycle*,[26−28] and aromatics undergo methylation and dealkylation in the *aromatics cycle*;[26,27,29,30] the two cycles are interconnected via dehydrocyclization of olefins to aromatics and dealkylation of aromatics to olefins.[26,27,31] The organic components of active chain carriers are ultimately transformed into highly unsaturated carbonaceous residues, i.e., polycylic aromatic hydrocarbons, resulting in chain carrier termination.[17,32−37]

Adjudication of mechanisms for chain carrier initiation has persisted since the initial proposal of carbene dimerization[38] to recent reports advocating either H^+-catalyzed carbonylation of a framework-bound methoxide to a framework-bound acetate,[18,19] insertion of formaldehyde (or its acetal) into a C−H bond of a methoxide bound to an extraframework aluminum species,[21] or water-assisted C−C coupling between methane and formaldehyde on a Brønsted acid−Lewis acid site pair.[22] Consensus on mechanistic concepts for chain carrier propagation finds its foundation in the "dual-cycle" scheme;[26] these concepts provide mechanistic rationale for the effects of catalyst properties (e.g., topology,[39,40] morphology,[41,42] and composition[43,44]) and reaction parameters (e.g., temperature,[45] time,[46] and cofeed identity and concentration[47−49]) on yields and selectivity. Mechanistic concepts for chain carrier termination have received less attention and remain primitive compared with those for the initiation and propagation phases. In this Account, we attempt to convey nascent mechanistic consensus on chain carrier termination by describing our results from mechanistic studies and providing examples of leveraging the acquired mechanistic insights to mitigate catalyst deactivation.

FORMALDEHYDE-MEDIATED CHAIN CARRIER TERMINATION

Current industrial processes deploying methanol-to-hydrocarbons catalysis use HSAPO-34,[50] a silicoaluminophosphate zeotype with CHA topology, as the solid acid catalyst.[4−6] The CHA topology features large cages (ca. 1 nm) connected via narrow apertures (ca. 0.4 nm);[10] the large cages accommodate the organic cocatalysts, and the narrow apertures restrict egress of large hydrocarbons to confer high selectivity to ethylene and propylene (ca. ≥80 %C). These topological features also render chain carrier termination fast and turnover numbers low (ca. 10^2−10^3) because inactive organic cocatalysts (polycyclic aromatic hydrocarbons) and their active precursors (methyl-substituted benzenes) remain entrained within the zeotype. We began probing the mechanism of chain carrier termination by examining the effects of process parameters on turnover number and selectivity.[51]

Turnover numbers for methanol-to-hydrocarbons catalysis on HSSZ-13,[52] the aluminosilicate analogue of HSAPO-34, decrease monotonically with both increasing initial methanol concentration ($P_{MeOH,0}$) and increasing space velocity (SV) (see Figure 1). These trends are consistent with the reported trend of decreasing turnover number with increasing space velocity for methanol-to-hydrocarbons catalysis on TON zeolites.[53] Reaction cascades for chain carrier termination, transforming active aromatic cocatalysts (methyl-substituted benzenes) to polycyclic aromatic hydrocarbons, must involve either alkylation or cycloaddition for C−C bond formation. Alkylation of methyl-substituted benzenes can involve either C_1 or $C_{\geq 2}$ coupling partners, while cycloaddition requires $C_{\geq 2}$ coreactants. The process parameters $P_{MeOH,0}$ and SV act on the concentrations of $C_{\geq 2}$ species in divergent directions but in the same direction on the concentrations of C_1 species. More specifically, the concentrations of $C_{\geq 2}$ species increase with increasing $P_{MeOH,0}$ and decreasing SV, while the concentrations of C_1 species increase with both increasing $P_{MeOH,0}$ and increasing SV. Taken together, the two trends in Figure 1 then suggest that chain carrier termination involves alkylation of active organic cocatalysts by a methanol-derived C_1 species.[54] We hypothesized that formaldehyde is this C_1 alkylating agent.

Methane selectivity increases with $P_{MeOH,0}$ and is nearly 100% at early times-on-stream in methanol-to-hydrocarbons catalysis on HSSZ-13 (Figure 2). These results, consistent with previous reports,[55−62] demonstrate that methanol engages in secondary transfer (de)hydrogenation reactions,

$$CH_3OH + C_nH_m \rightarrow CH_4 + H_2O + C_nH_{m-2} \quad (1)$$

$$CH_3OH + C_nH_m \rightarrow HCHO + C_nH_{m+2} \quad (2)$$

and primary disproportionation to give methane and formaldehyde,[56,59,60,63]

DOI: 10.1021/acs.accounts.9b00204
Acc. Chem. Res. 2019, 52, 2647−2656

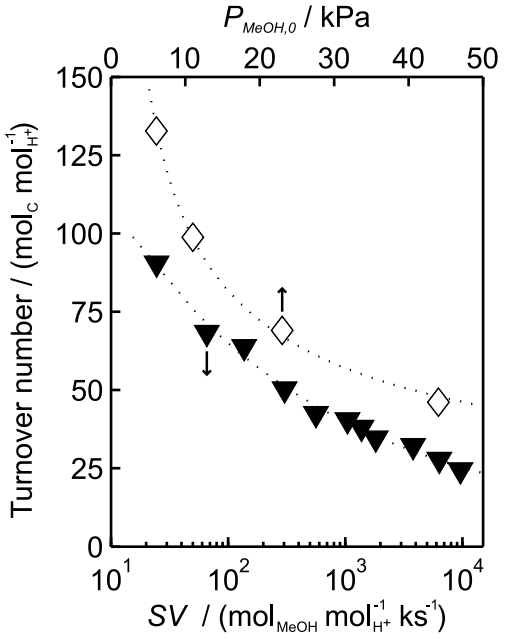

Figure 1. Turnover number vs space velocity (SV) (bottom abscissa, solid triangles; $P_{MeOH,0}$ = 22 kPa) and influent methanol partial pressure ($P_{MeOH,0}$) (top abscissa, open diamonds; SV = 63 mol_{MeOH} $mol_{H^+}^{-1}$ ks^{-1}) for methanol-to-hydrocarbons reactions at 623 K on HSSZ-13 (Si/Al = 8.4, 1.2 × 10^{-3} mol_{H^+} g^{-1}). The dotted lines are guides for the eye.

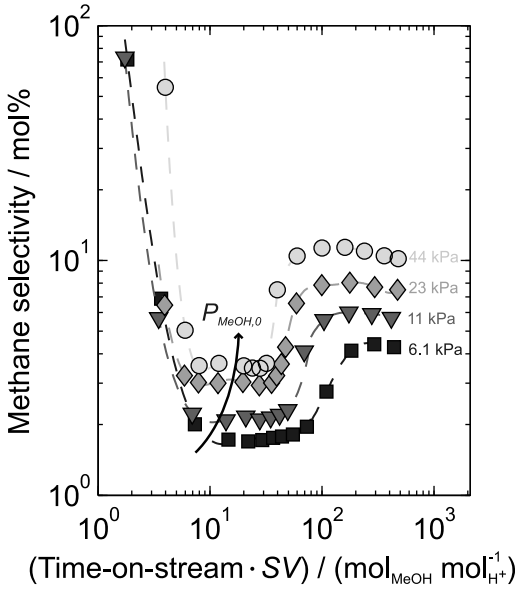

Figure 2. Methane selectivity vs time-on-stream normalized by inverse space velocity during methanol-to-hydrocarbons reactions at 623 K and SV = 63 mol_{MeOH} $mol_{H^+}^{-1}$ ks^{-1} on HSSZ-13 (Si/Al = 8.4, 1.2 × 10^{-3} mol_{H^+} g^{-1}) with influent methanol partial pressures ($P_{MeOH,0}$) of 6.1 kPa (squares), 11 kPa (triangles), 23 kPa (diamonds), and 44 kPa (circles). The dashed lines are guides for the eye.

$$CH_3OH + CH_3OH \rightarrow HCHO + CH_4 + H_2O \quad (3)$$

We did not observe formaldehyde in the reactor effluent, but others[58,61,62] detected formaldehyde during methanol reactions at low conversions on MFI,[58,61,64] FAU,[58] and CHA[62] formulations. We proposed that under the examined reaction conditions, formaldehyde is scavenged rapidly by active organic cocatalysts to instigate their maturation (olefinic to aromatic) and/or termination (aromatic to polycyclic aromatic) (see Scheme 2). Formaldehyde reacts with olefins in acidic media via Prins condensation[65] to give dienes and with aromatics to give products mediated by benzyl carbenium ions.[63] Examples of these formaldehyde reactions on solid acids include condensation of isobutene with formaldehyde to form isoprene on alumino- and borosilicates[66] and condensation of benzene with formaldehyde to give diarylmethane on large-pore zeolites.[67] The possible nucleophiles that can attack benzyl carbenium ions include both olefins and aromatics in methanol-to-hydrocarbons catalysis on medium- and large-pore zeolites but only olefins for methanol-to-hydrocarbons catalysis on small-pore zeolites that prevent intercage diffusion of bulky aromatics. We pursued corroboration of the chain carrier termination pathways proposed in Scheme 2 by examining differences in turnover number and conversion transients for methanol versus dimethyl ether reactions.

Figure 3a shows conversion versus time on stream normalized by inverse space velocity for methanol reaction and dimethyl ether reaction on HSAPO-34. The areas under these curves equal the turnover numbers for the respective reactions. The turnover number is approximately 5 times larger in the dimethyl ether reaction (330 mol_C $mol_{H^+}^{-1}$) than in the methanol reaction (62 mol_C $mol_{H^+}^{-1}$). Furthermore, the time-on-stream derivative of conversion reaches a higher maximum and lower minimum in the methanol reaction compared with the dimethyl ether reaction (Figure 3b). If conversion reflects a rate of hydrocarbon production, which is necessarily proportional to the number of active chain carriers, then the magnitude of the time-on-stream derivative of conversion reflects the *acceleration* and *deceleration* of hydrocarbon production, i.e., the rates of chain carrier initiation and termination, respectively. The more positive *acceleration* and more negative *deceleration* with $P_{MeOH,0}$ (see Figure 4) comport with the supposition that these metrics reflect rates of chain carrier initiation and termination. These results on the effect of feedstock identity on catalyst deactivation are consistent with a previous report comparing methanol and dimethyl ether reactions on HSAPO-34.[68] We assert that these differences in turnover number and rate of chain carrier termination are manifestations of differences in the faculty to engage in tranfer (de)hydrogenation reactions between methanol and dimethyl ether. Methanol undergoes rapid bimolecular dehydration to form dimethyl ether,

$$CH_3OH + CH_3OH \rightarrow CH_3OCH_3 + H_2O \quad (4)$$

on solid acids under reaction conditions typical for methanol-to-hydrocarbons catalysis.[11,27,38,40,69,70] Methanol disproportionation and dehydration (eqs 3 and 4, respectively) thus constitute the primary reactions in methanol-to-hydrocarbons catalysis. Dimethyl ether cannot undergo an analogous disproportionation reaction, as there exists no stable product of dimethyl ether dehydrogenation, and similarly, there exists no analogue of methanol transfer dehydrogenation (eq 2) for dimethyl ether. Thus, to access formaldehyde-mediated chain carrier termination pathways (Scheme 2), dimethyl ether must first engage in a methylation event, e.g.,

$$CH_3OCH_3 + H^+ \rightarrow CH_3OH + CH_3^+$$

DOI: 10.1021/acs.accounts.9b00204
Acc. Chem. Res. 2019, 52, 2647−2656

Scheme 2. Transfer Dehydrogenation of Methanol To Give Formaldehyde and Alkylation of Olefins and Aromatics by Formaldehyde

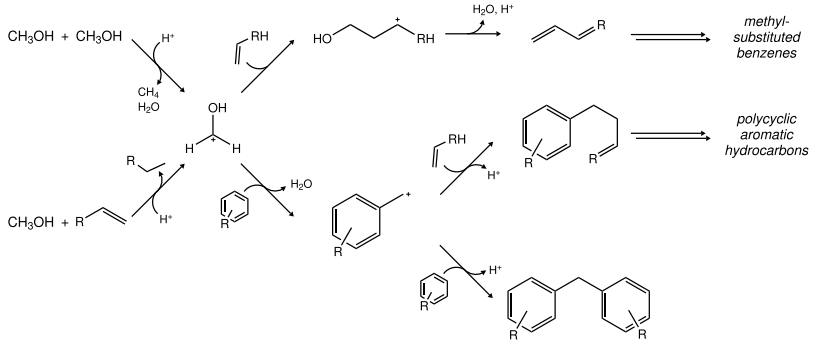

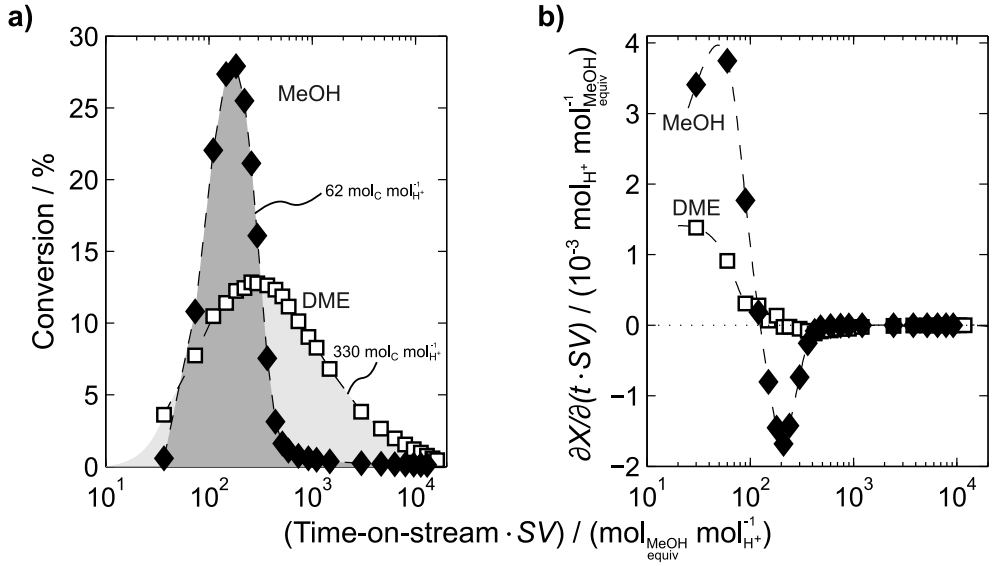

Figure 3. (a) Conversion (X) and (b) time-on-stream derivative of conversion ($\partial X/\partial(t{\cdot}\mathrm{SV})$) vs time-on-stream normalized by inverse space velocity during methanol reaction (MeOH, solid diamonds; 44 kPa) and dimethyl ether reaction (DME, open squares; 21 kPa) on HSAPO-34 at 623 K and SV = 1.2 × 10^3 $\mathrm{mol_{MeOH\ equiv}\ mol_{H^+}^{-1}\ ks^{-1}}$. The dashed and dotted lines are guides for the eye.

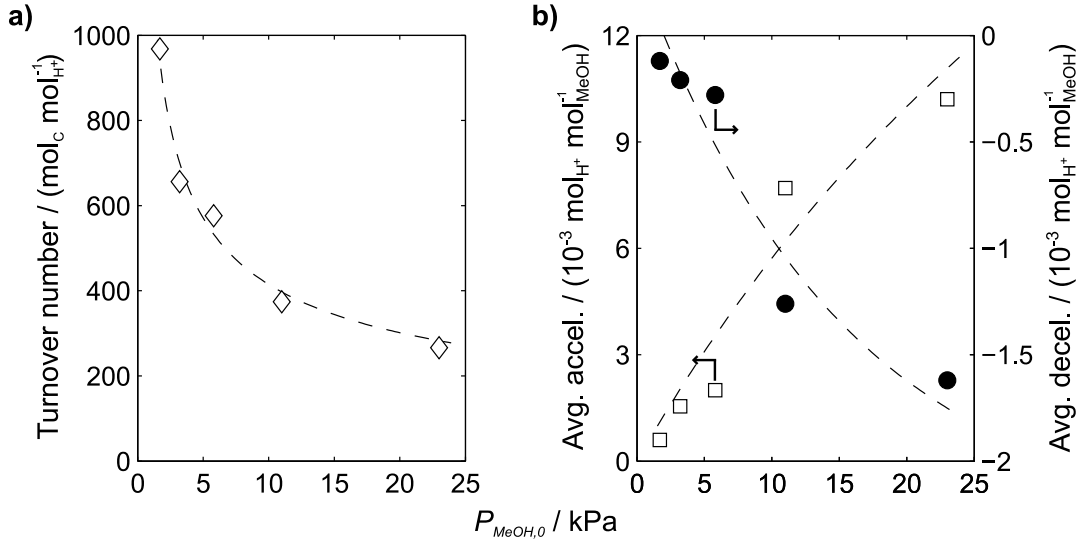

Figure 4. (a) Turnover number and (b) average acceleration (open squares, left ordinate) and average deceleration (solid circles, right ordinate) vs influent methanol partial pressure ($P_{\mathrm{MeOH},0}$) for methanol-to-hydrocarbons reactions on HSAPO-34 at 673 K and 1.2 × 10^2 $\mathrm{mol_{MeOH}\ mol_{H^+}^{-1}\ ks^{-1}}$. Average acceleration values are arithmetic means of time-on-stream derivatives of the conversion at times-on-stream before the initial inflection point, and average deceleration values are arithmetic means of time-on-stream derivatives of conversion at times-on-stream between the critical point and the second inflection point. The dashed lines are guides for the eye.

DOI: 10.1021/acs.accounts.9b00204
Acc. Chem. Res. 2019, 52, 2647−2656

or hydrolysis (i.e., the reverse of eq 4) to form methanol, which then must undergo transfer dehydrogenation. We pursued further corroboration of the formaldehyde reactions proposed in Scheme 2 by examining trends in steady-state selectivity with $P_{MeOH,0}$ and formaldehyde cofeed concentration ($P_{HCHO,0}$) in methanol-to-hydrocarbons catalysis on MFI zeolites.[44]

The MFI topology features a network of intersecting medium-pore (ca. 0.5−0.6 nm) channels[10] that enable ingress and egress of aromatic cocatalysts. These topological features render chain carrier termination slow, permitting evaluation of steady-state conversion and selectivity.[11,27,40] Steady-state selectivity in methanol-to-hydrocarbons catalysis on MFI zeolites reflects the prevailing steady-state composition of the organic cocatalysts.[41−43,45,47,49] Ethylene is a product predominantly of the aromatics cycle while propylene is a product of both the olefins cycle and the aromatics cycle.[26,47] An increase in ethylene selectivity simultaneous with a decrease in propylene selectivity thus reflects an increase in population of aromatic cocatalysts relative to olefinic cocatalysts.

Table 1 lists the conversions and selectivities for methanol reactions on HMFI with varying $P_{MeOH,0}$ and $P_{HCHO,0}$. The propylene selectivity decreases monotonically with both $P_{MeOH,0}$ and $P_{HCHO,0}$, and the selectivities for ethylene and methyl-substituted benzenes (MBs) both increase monotonically with both $P_{MeOH,0}$ and $P_{HCHO,0}$. These selectivity trends are consistent with the pathways proposed in Scheme 2 for formaldehyde-mediated dehydrocyclization of olefins to aromatics. The concentration of formaldehyde local to chain carriers increases with both $P_{MeOH,0}$ and $P_{HCHO,0}$, resulting in higher rates of formaldehyde-mediated aromatization. This shifts the population of organic cocatalysts, depleting olefins in favor of aromatics, with commensurate decrease in propylene selectivity and increase in ethylene selectivity.

Table 1. Steady-State Conversions and Selectivities for Methanol Reactions with and without Formaldehyde Cofeed on HMFI at 673 K

			selectivity[a]/%C		
$P_{MeOH,0}$/kPa	$P_{HCHO,0}$/Pa	conv./%	C_3[b]	C_2[c]	MBs[d]
0.6	0	30	42	1.5	0.1
2.5	0	32	38	1.9	2.1
13	0	35	35	2.9	2.6
53	0	30	29	9.8	5.9
0.6	0	30	42	1.5	0.1
0.6	3.0	36	38	2.7	1.6
0.6	10	40	36	7.2	5.7
0.6	20	22	26	21	17

[a]The balance of selectivity is ascribed to C_{4+} aliphatic hydrocarbons. [b]Propylene + propane, propylene:propane ≥99:1. [c]Ethylene + ethane, ethylene:ethane ≥99:1. [d]Methyl-substituted benzenes.

The results in Figures 1−4 and Table 1 are consistent with the results of Lercher and co-workers[71−73] regarding methanol-to-hydrocarbons catalysis on HMFI. They attributed (i) the decrease in deactivation rate with increasing ratio of cofed *n*-butanol to methanol in the reactor influent,[71] (ii) the decrease in deactivation rate with a back-mixed reactor versus a plug-flow reactor,[72] and (iii) the discontinuity in the rate of formation of saturated hydrocarbons with space velocity[73] to a "methanol-induced hydride transfer" pathway.[73] They proposed[73] a formaldehyde-mediated pathway for aromatization of olefins that comports conceptually with the reactions in Scheme 2: formaldehyde formed via transfer dehydrogenation of methanol engages with olefins in Prins condensation to give dienes that then undergo dehydrocyclization.

Scheme 2 also finds corroboration from archived reports from Olsbye and co-workers[74−76] comparing catalyst deactivation rates and selectivities in methanol reactions versus dimethyl ether reactions on medium- and large-pore zeolites and zeotypes. MFI and AFI zeolites and zeotypes deactivate faster during methanol reactions than during dimethyl ether reactions, consistent with results on CHA formulations[68] (Figure 3). Diarylmethane forms in the coreaction of benzene and methanol but not in the coreaction of benzene and dimethyl ether; this result supports the notion that formaldehyde is formed in methanol reactions but not in dimethyl ether reactions and provides corroboration for the aromatic alkylation reactions depicted in Scheme 2. The rates of both isobutane and aromatics formation increase with increasing fraction of methanol in the reactions of mixtures of isobutene, methanol, and dimethyl ether on MFI zeolites, consistent with the formaldehyde-mediated pathways for olefin aromatization depicted in Scheme 2.

We next discuss strategies to prolong catalyst lifetime by circumventing or otherwise mitigating formaldehyde-mediated chain carrier termination.

MITIGATING CHAIN CARRIER TERMINATION

Additional Function for Selective Formaldehyde Removal

The turnover numbers for methanol-to-hydrocarbons catalysis on CHA zeolites and zeotype increase upon physical addition of rare-earth oxides without disrupting the high selectivity to ethylene and propylene.[78−80] Figure 5a shows turnover numbers for reactions on HSAPO-34/HSSZ-13, an *inter*pellet mixture of HSAPO-34/HSSZ-13 and Y_2O_3 aggregates, and an *intra*pellet mixture, i.e., aggregates composed of well-mixed HSAPO-34/HSSZ-13 and Y_2O_3 powders. Figure 5a also shows the "relative change in turnover number", defined as the turnover number for a given reaction normalized by the turnover number for the reaction with only the zeotype/zeolite. The turnover numbers increase 2-fold with loose interpellet mixtures and 4-fold for intimate intraparticle mixtures. This proximity effect[81] implies that a species formed within the solid acid egresses through the narrow apertures of the zeotype/zeolite, enters the bulk fluid phase, and is transported to the Y_2O_3 surface, where it is adsorbed, consumed, or otherwise rendered innocuous to catalyst lifetime. Formaldehyde matches the criteria prescribed by this proximity effect.

Surfaces of irreducible rare-earth oxides expose sites that function like bases.[82−87] Reactions of formaldehyde with water on Y_2O_3 under conditions distinct from those for methanol-to-hydrocarbons catalysis (i.e., $T \leq 573$ K and $P_{HCHO} > 0.1$ kPa) produce methanol and CO_2 in a 2:1 molar ratio via a reaction cascade of disproportionation to give methanol and formic acid followed by decarboxylative transfer hydrogenation to form methanol and CO_2.[88] The disproportionation reaction is reminiscent of the Cannizarro reaction for aldehyde disproportionation in aqueous basic media[89] and on alkaline-earth oxides,[90] confirming that the catalytic sites exposed on Y_2O_3 surfaces indeed function as bases in formaldehyde reactions. Formaldehyde reactions on Y_2O_3 under conditions resembling those for methanol-to-hydrocarbons catalysis (i.e., $T \geq 673$ K

DOI: 10.1021/acs.accounts.9b00204
Acc. Chem. Res. 2019, 52, 2647−2656

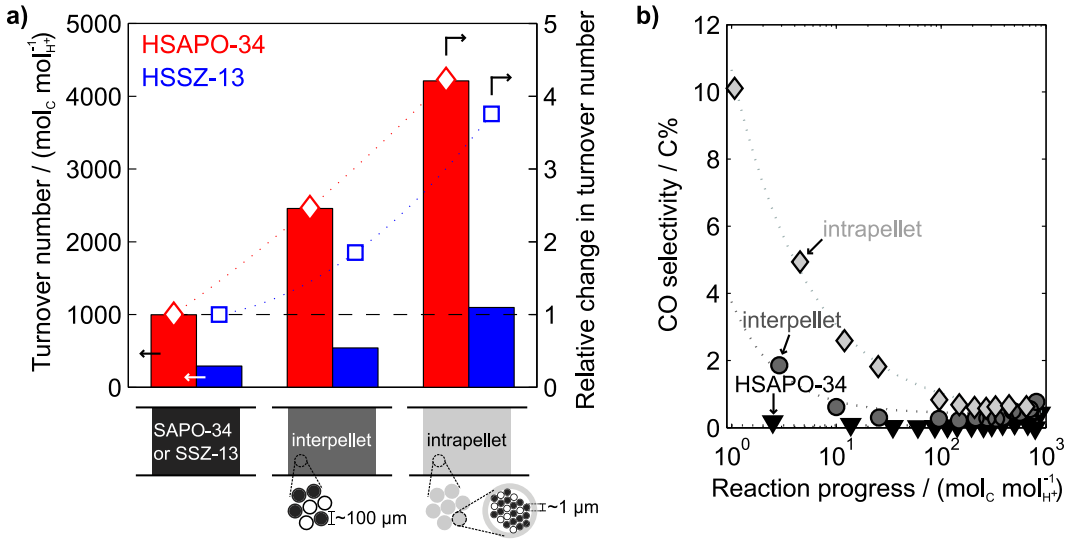

Figure 5. (a) Turnover number (left ordinate, bars) and relative change in turnover number (right ordinate, diamonds and squares) for methanol-to-hydrocarbons reactions on HSAPO-34/HSSZ-13, an interpellet physical mixture of HSAPO-34/HSSZ-13 with Y_2O_3, and an intrapellet physical mixture of HSAPO-34/HSSZ-13 with Y_2O_3. (b) CO selectivity for methanol-to-hydrocarbons reactions on HSAPO-34 (triangles), an interpellet physical mixture of HSAPO-34 with Y_2O_3 (circles), and an intrapellet physical mixture of HSAPO-34 with Y_2O_3 (diamonds) vs reaction progress.[77] Reaction conditions: 673 K, 12 kPa MeOH, 24 wt % Y_2O_3, and 1.2×10^2 mol_{MeOH} $mol_{H^+}^{-1}$ ks^{-1}. The dotted lines are guides for the eye.

and P_{HCHO} < 0.1 kPa) instead produce CO with high selectivity (≥90%) and yield (≥70%).[80] Apparently, monomolecular formaldehyde decarbonylation is favored over bimolecular formaldehyde disproportionation at the higher temperatures and lower formaldehyde concentrations relevant to methanol-to-hydrocarbons catalysis.

CO is formed in only negligible quantities during methanol-to-hydrocarbons reactions on HSAPO-34 but in measurable quantities for reactions with added Y_2O_3 (Figure 5b). The base sites exposed on the Y_2O_3 surface scavenge formaldehyde via decomposition, thereby mitigating formaldehyde-mediated chain carrier termination and increasing catalyst lifetime. Scheme 3 summarizes the formaldehyde reactions in this bifunctional system. Transfer dehydrogenation of methanol by, e.g., an olefin produces formaldehyde in the zeotype/zeolite domain (z). Formaldehyde in the zeotype/zeolite domain can react with olefinic or aromatic chain carriers to instigate their maturation or termination, respectively, via the reactions depicted in Scheme 2. Formaldehyde can instead diffuse out of the zeotype/zeolite and into the bulk fluid phase (g) and, once in the fluid phase, can be transported into the domain of the rare-earth oxide (reo) and undergo decomposition. The discrepancies in CO selectivity and turnover number between the inter- and intrapellet mixtures show that the rate of formaldehyde decomposition (step (6) in Scheme 3) depends on mixture intimacy. This proximity effect implies that formaldehyde concentration gradients persist at pellet and crystallite length scales (ca. 10^2 and 10^0 μm, respectively), i.e., the rates of steps (2) and (3) in Scheme 3 are larger than or similar in magnitude to the overall net rate of steps (4) and (5).

Scheme 3. Chemical Reactions and Physical Transport Steps Involving Formaldehyde in Bifunctional Methanol-to-Hydrocarbons Catalysis on Zeotypes/Zeolites and Basic Metal Oxides

$$CH_3OH\,(z) + C_nH_{2n}\,(z) \rightarrow HCHO\,(z) + C_nH_{2n+2}\,(z) \quad (1)$$

$$HCHO\,(z) + \text{olefin}\,(z) \Rightarrow \text{aromatic}\,(z) \quad (2)$$

$$HCHO\,(z) + \text{aromatic}\,(z) \Rightarrow \text{polycyclic aromatic hydrocarbon}\,(z) \quad (3)$$

$$HCHO\,(z) \rightleftharpoons HCHO\,(g) \quad (4)$$

$$HCHO\,(g) \rightleftharpoons HCHO\,(reo) \quad (5)$$

$$HCHO\,(reo) \rightarrow CO\,(g) + H_2\,(g) \quad (6)$$

Bifunctional formulations with nanoscale proximity between H^+ sites and sites for selective formaldehyde removal would obviate the kinetic relevance of interphase transport steps (steps (4) and (5) in Scheme 3) intervening formaldehyde formation and formaldehyde removal. Nanoparticles of rare-earth oxides encapsulated within CHA zeotypes and zeolites thus represent interesting though likely challenging targets for synthesis; the scope of demonstrated techniques to encapsulate oxides within small-pore zeotypes/zeolites remains limited.[91−93] Studies elaborating the structural and site requirements of oxides for selective formaldehyde decomposition should precede such synthetic endeavors to ensure that high selectivity and yields can be obtained on rare-earth oxide nanoparticles and/or supported, well-dispersed rare-earth oxo moieties. Exploring alternative functions for selective formaldehyde removal, e.g., selective C=O versus C=C hydrogenation, is another interesting pursuit, especially if this function can be encapsulated within zeotype/zeolite crystals.

Sacrificial Hydrogen Donors

The turnover numbers for methanol-to-hydrocarbons catalysis on HSAPO-34 increase monotonically with increasing hydrogen pressure—from a 3-fold increase at 4 bar H_2 relative to the reaction without added H_2 to a >70-fold[94] increase at 30 bar H_2[95] (Figure 6). The selectivity to C_2-C_4 aliphatic products remains high (>85 C%) regardless of the H_2 pressure, but the fraction of olefins within the C_2-C_4 products decreases monotonically from 98 mol % without added H_2 to 92 mol % at 30 bar H_2. The increase in C_2-C_4 paraffin selectivity and commensurate decrease in C_2-C_4 olefin selectivity suggest that HSAPO-34 effects C=C hydrogenation. Archived reaction energetics computed using ab initio methods suggest that olefin hydrogenation reactions on H^+-form zeolites are

DOI: 10.1021/acs.accounts.9b00204
Acc. Chem. Res. 2019, 52, 2647−2656

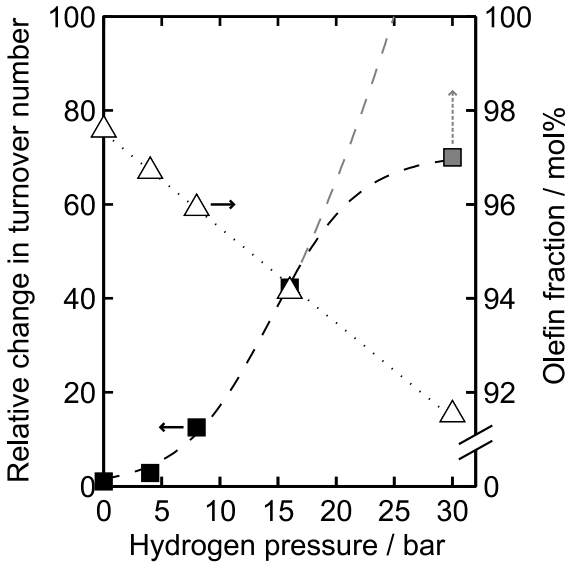

Figure 6. Relative change in turnover number (left, solid squares) and olefin fraction (right, open triangles) vs hydrogen pressure for methanol-to-hydrocarbons reactions on HSAPO-34 at 673 K, 13 kPa MeOH, and 3.1×10^2 mol_{MeOH} $mol_{H^+}^{-1}$ ks^{-1}. The dashed and dotted lines are guides for the eye.[94]

kinetically accessible,[96] and the fidelity of measured rate constants for both alkane dehydrogenation and alkene hydrogenation to the principle of microscopic reversibility and De Donder formalisms provides experimental verification.[97] A plausible explanation for the effects of H_2 on lifetime and selectivity in methanol-to-hydrocarbons catalysis supposes that high H_2 pressures enable hydrogenation of C=C bonds within intermediates formed along the cascade of reactions for aromatization—e.g., dienes or alkenyl-substituted aromatics—to attenuate chain carrier maturation and termination. This supposition is corroborated by kinetic studies showing that second-order rate constants for 1,3-butadiene hydrogenation on H^+-form CHA, AEI, FER, and BEA zeolites are ca. 10^2 times larger than those for ethylene and propylene hydrogenation.[98]

Another plausible explanation invokes the intrinsic selectivity of H^+-form zeolites and zeotypes for C=O over C=C hydrogenation. Senger and Radom[96] computed energetics for formaldehyde and ethylene hydrogenation trajectories on a three-T-atom aluminosilicate cluster at 0 K. The energy difference between the transition state and the reactant (gas-phase species plus the bare three-T-atom cluster) is ca. 100 kJ mol^{-1} lower for formaldehyde hydrogenation versus ethylene hydrogenation. High H_2 pressures perhaps render both C=O and C=C hydrogenation kinetically accessible to suppress formaldehyde-mediated chain carrier termination pathways by hydrogenating formaldehyde to methanol and olefinic moieties to their saturated analogues.

Another plausible explanation considers H_2-mediated cleavage of C−C bonds within carbonaceous deposits on H^+-form zeolites. Jong et al.[99] examined the efficacy of thermal treatments under H_2 to regenerate HMFI deactivated by the formation of carbonaceous deposits in ethylbenzene reactions. They examined HMFI before reaction, after deactivation in reaction of ethylbenzene at 603 K, and after subsequent thermal treatment in flowing H_2 at 773 K using thermogravimetric analysis, infrared spectroscopy, ^{13}C magic-angle spinning (MAS) spectroscopy, and Xe equilibrium adsorption and ^{129}Xe MAS NMR spectroscopy. The H_2 regeneration protocol partially regenerated the catalyst (15% conversion for the fresh catalyst vs 10% upon regeneration), reduced the mass of carbonaceous deposits by 38%, decreased the band intensity for aliphatic C−H stretches and increased the band intensity for the Brønsted O−H stretch while leaving the band intensity for aromatic C−H stretches unchanged, decreased the area of ^{13}C resonances in the region for alkyl chemical shifts while retaining the area of resonances for aromatics, and recovered 80% of the micropore volume accessible to Xe. These results suggest that monofunctional H^+-form zeolites promote H_2-mediated aromatic dealkylation reactions typically encountered in bifunctional metal-acid hydrocracking.[100] High H_2 pressures perhaps facilitate dealkylation of alkenyl-substituted aromatics and species derived therefrom to prevent chain carrier termination.

The scope of this strategy can perhaps be broadened to alternative hydrogen donors[101,102] and/or alternative reactions for C=C and C=O saturation.[103] More potent and more selective hydrogen donors would reduce operating costs associated with hydrogen compression without further burdening the already energy-intensive olefin/paraffin separations. Alkylation by alkanes for saturation of olefinic and carbonyl moieties instead of hydrogenation by H_2 (i.e., addition of C−H instead of H−H across C=C and C=O) would provide means to valorize low-value, distressed alkane streams.

■ CONCLUDING REMARKS

Formaldehyde formed via transfer dehydrogenation of methanol accelerates chain carrier termination in methanol-to-hydrocarbons catalysis on zeotypes and zeolites. Formaldehyde engages with active chain carriers in alkylation reactions to instigate cascades of successive transfer dehydrogenation steps that result in termination of the once-active chain carriers. Strategies to circumvent formaldehyde-mediated chain carrier termination include introducing additional catalytic functions and coprocessing sacrificial hydrogen donors to scavenge formaldehyde and/or intercept intermediates along dehydrocyclization cascades. These mechanistic results and mitigation strategies provide cause to (re)consider solid acids previously disregarded for their rapid deactivation and realize the full spectrum of shape selectivity afforded by the catalogue of zeolite/zeolite structures. Circumventing chain carrier termination also obviates the need for operation of fluidized-bed reactors in the industrial deployment of this catalysis, thereby relaxing constraints imposed on process parameters and catalyst properties that were otherwise optimized in part to avoid attrition and maintain fluidization of catalyst formulations. We envision the utility of these mechanistic concepts to extend beyond methanol-to-hydrocarbons catalysis to affect other applications of acid catalysis where hydrogen transfer and coking reactions prevail to restrict catalyst stability, and we also find prospects to leverage the consequences of formaldehyde-mediated dehydrocyclization in developing catalysis for selective and robust C_1 aromatization.

■ AUTHOR INFORMATION

Corresponding Authors

*E-mail: andrew.hwang@honeywell.com.
*E-mail: abhan@umn.edu.

DOI: 10.1021/acs.accounts.9b00204
Acc. Chem. Res. 2019, 52, 2647−2656

ORCID

Aditya Bhan: 0000-0002-6069-7626

Present Address

‡A.H.: Exploratory Research, Honeywell UOP, Des Plaines, IL 60017, USA.

Notes

The authors declare no competing financial interest.

Biographies

Andrew Hwang is a research scientist at Honeywell UOP in Des Plaines, IL. He received a B.S. in Chemical and Biomolecular Engineering from UC Berkeley in 2013 and a Ph.D. in Chemical Engineering from the University of Minnesota in 2018.

Aditya Bhan received his Bachelor of Technology (B.Tech.) in Chemical Engineering from IIT Kanpur in 2000 and his Ph.D. in Chemical Engineering from Purdue University in 2005. From January 2005 to August 2007 he was a postdoctoral scholar at the University of California at Berkeley, and since then he has been on the Chemical Engineering and Materials Science faculty at the University of Minnesota, where he currently serves as the Shell Chair Professor in Chemical Engineering. He leads a research group that focuses on mechanistic characterization of catalysts useful in energy conversion and petrochemical synthesis. His group at the University of Minnesota has been recognized with the Young Researcher Award from the Acid–Base Catalysis Society, the Ipatieff Prize from the American Chemical Society, the Early Career Award from the U.S. Department of Energy, and the NSF Career Award. He serves as Associate Editor for the *Journal of Catalysis*.

■ ACKNOWLEDGMENTS

We gratefully acknowledge support from Dow through the University Partnership Initiative and the National Science Foundation (CBET 1701534). We also acknowledge Rachit Khare, Dario Prieto-Centurion, Sukaran Arora, Praveen Bollini, Brandon Foley, and Zhichen Shi for their contributions to the research predicating this Account.

■ REFERENCES

(1) Olah, G. A.; Goeppert, A.; Surya Prakash, G. K. *Beyond Oil and Gas: The Methanol Economy*, 3rd ed.; John Wiley & Sons, 2018.

(2) van Bekkum, H.; Flanigen, E. M.; Jacobs, P. A.; Jansen, J. C. *Introduction to Zeolite Science and Practice*, 2nd ed.; Elsevier, 2001.

(3) Čejka, J.; Corma, A.; Zones, S. *Zeolites and Catalysis: Synthesis, Reactions and Applications*; John Wiley & Sons, 2010.

(4) Vora, B. V.; Marker, T. L.; Barger, P. T.; Nilsen, H. R.; Kvisle, S.; Fuglerud, T. Economic route for natural gas conversion to ethylene and propylene. *Stud. Surf. Sci. Catal.* **1997**, *107*, 87–98.

(5) Tian, P.; Wei, Y.; Ye, M.; Liu, Z. Methanol to Olefins (MTO): From Fundamentals to Commercialization. *ACS Catal.* **2015**, *5*, 1922–1938.

(6) Xie, Z.; Liu, J.; Yang, W.; Zhong, S.; Chen, X. Process for producing lower olefins from methanol or dimethyl ether. U.S. Patent 7,692,056 B2, 2010.

(7) Centi, G.; Quadrelli, E. A.; Perathoner, S. Catalysis for CO_2 conversion: A key technology for rapid introduction of renewable energy in the value chain of chemical industries. *Energy Environ. Sci.* **2013**, *6*, 1711–1731.

(8) Goeppert, A.; Czaun, M.; Jones, J.-P.; Surya Prakash, G. K.; Olah, G. A. Recycling of carbon dioxide to methanol and derived products – closing the loop. *Chem. Soc. Rev.* **2014**, *43*, 7995–8048.

(9) Sheldon, R. A. Green chemistry, catalysis and valorization of waste biomass. *J. Mol. Catal. A: Chem.* **2016**, *422*, 3–12.

(10) Baerlocher, C.; McCusker, L. B.; Olson, D. H. *Atlas of Zeolite Framework Types*, 6th ed.; Elsevier, 2007.

(11) Haw, J. F.; Song, W.; Marcus, D. M.; Nicholas, J. B. The Mechanism of Methanol to Hydrocarbon Catalysis. *Acc. Chem. Res.* **2003**, *36*, 317–326.

(12) Olah, G. A.; Surya Prakash, G. K.; Ellis, R. W.; Olah, J. A. Remarks on the mechanism of ethylene formation from methyl alcohol. *J. Chem. Soc., Chem. Commun.* **1986**, 9–10.

(13) Song, W.; Marcus, D. M.; Fu, H.; Ehresmann, J. O.; Haw, J. F. An Oft-Studied Reaction That May Never Have Been: Direct Catalytic Conversion of Methanol or Dimethyl Ether to Hydrocarbons on the Solid Acids HZSM-5 or HSAPO-34. *J. Am. Chem. Soc.* **2002**, *124*, 3844–3845.

(14) Jiang, Y.; Wang, W.; Reddy Marthala, V. R.; Huang, J.; Sulikowski, B.; Hunger, M. Effect of organic impurities on the hydrocarbon formation via the decomposition of surface methoxy groups on acidic zeolite catalysts. *J. Catal.* **2006**, *238*, 21–27.

(15) Lesthaeghe, D.; Van Speybroeck, V.; Marin, G. B.; Waroquier, M. Understanding the Failure of Direct C–C Coupling in the Zeolite-Catalyzed Methanol-to-Olefin Process. *Angew. Chem., Int. Ed.* **2006**, *45*, 1714–1719.

(16) Marcus, D. M.; McLachlan, K. A.; Wildman, M. A.; Ehresmann, J. O.; Kletnieks, P. W.; Haw, J. F. Experimental Evidence from H/D Exchange Studies for the Failure of Direct C–C Coupling Mechanisms in the Methanol-to-Olefin Process Catalyzed by HSAPO-34. *Angew. Chem., Int. Ed.* **2006**, *45*, 3133–3136.

(17) Olsbye, U.; Svelle, S.; Lillerud, K. P.; Wei, Z. H.; Chen, Y. Y.; Li, J. F.; Wang, J. G.; Fan, W. B. The formation and degradation of active species during methanol conversion over protonated zeotype catalysts. *Chem. Soc. Rev.* **2015**, *44*, 7155–7176.

(18) Liu, Y.; Müller, S.; Berger, D.; Jelic, J.; Reuter, K.; Tonigold, M.; Sanchez-Sanchez, M.; Lercher, J. A. Formation Mechanism of the First Carbon-Carbon Bond and the First Olefin in the Methanol Conversion into Hydrocarbons. *Angew. Chem., Int. Ed.* **2016**, *55*, 5723–5726.

(19) Chowdhury, A. D.; Houben, K.; Whiting, G. T.; Mokhtar, M.; Asiri, A. M.; Al-Thabaiti, S. A.; Basahel, S. N.; Baldus, M.; Weckhuysen, B. M. Initial Carbon-Carbon Bond Formation during the Early Stages of the Methanol-to-Olefin Process Proven by Zeolite-Trapped Acetate and Methyl Acetate. *Angew. Chem., Int. Ed.* **2016**, *55*, 15840–15845.

(20) Plessow, P. N.; Studt, F. Unraveling the Mechanism of the Initiation Reaction of the Methanol to Olefins Process Using ab Initio and DFT Calculations. *ACS Catal.* **2017**, *7*, 7987–7994.

(21) Wang, C.; Chu, Y.; Xu, J.; Wang, Q.; Qi, G.; Gao, P.; Zhou, X.; Deng, F. Extra-Framework Aluminum-Assisted Initial C–C Bond Formation in Methanol-to-Olefins Conversion on Zeolite H-ZSM-5. *Angew. Chem., Int. Ed.* **2018**, *57*, 10197–10201.

(22) Chu, Y.; Yi, X.; Li, C.; Sun, X.; Zheng, A. Brønsted/Lewis acid sites synergistically promote the initial C–C bond formation in the MTO reaction. *Chem. Sci.* **2018**, *9*, 6470–6479.

(23) Dahl, I. M.; Kolboe, S. On the reaction mechanism for propene formation in the MTO reaction over SAPO-34. *Catal. Lett.* **1993**, *20*, 329–336.

(24) Dahl, I. M.; Kolboe, S. On the reaction mechanism for hydrocarbon formation from methanol over SAPO-34. 1. Isotopic labeling studies of the co-reaction of ethene and methanol. *J. Catal.* **1994**, *149*, 458–464.

(25) Dahl, I. M.; Kolboe, S. On the reaction mechanism for hydrocarbon formation from methanol over SAPO-34. 2. Isotopic labeling studies of the co-reaction of propene and methanol. *J. Catal.* **1996**, *161*, 304–309.

(26) Svelle, S.; Joensen, F.; Nerlov, J.; Olsbye, U.; Lillerud, K.-P.; Kolboe, S.; Bjørgen, M. Conversion of Methanol into Hydrocarbons over Zeolite H-ZSM-5: Ethene Formation Is Mechanistically Separated from the Formation of Higher Alkenes. *J. Am. Chem. Soc.* **2006**, *128*, 14770–14771.

(27) Ilias, S.; Bhan, A. Mechanism of the Catalytic Conversion of Methanol to Hydrocarbons. *ACS Catal.* **2013**, *3*, 18–31.

DOI: 10.1021/acs.accounts.9b00204
Acc. Chem. Res. 2019, 52, 2647–2656

(28) Dessau, R. M. On the H-ZSM-5 Catalyzed Formation of Ethylene from Methanol or Higher Olefins. *J. Catal.* **1986**, *99*, 111−116.
(29) Song, W.; Haw, J. F.; Nicholas, J. B.; Heneghan, C. S. Methylbenzenes are the organic reaction centers for methanol-to-olefin catalysis on HSAPO-34. *J. Am. Chem. Soc.* **2000**, *122*, 10726−10727.
(30) Arstad, B.; Kolboe, S. The reactivity of molecules trapped within the SAPO-34 cavities in the methanol-to-hydrocarbons reaction. *J. Am. Chem. Soc.* **2001**, *123*, 8137−8138.
(31) Dejaifve, P.; Védrine, J. C.; Bolis, V.; Derouane, E. G. Reaction pathways for the conversion of methanol and olefins on H-ZSM-5 zeolite. *J. Catal.* **1980**, *63*, 331−345.
(32) Fu, H.; Song, W.; Haw, J. F. Polycyclic aromatics formation in HSAPO-34 during methanol-to-olefin catalysis: Ex situ characterization after cryogenic grinding. *Catal. Lett.* **2001**, *76*, 89−94.
(33) Mores, D.; Stavitski, E.; Kox, M. H. F.; Kornatowski, J.; Olsbye, U.; Weckhuysen, B. M. Space- and Time-Resolved in-Situ Spectroscopy on the Coke Formation in Molecular Sieves: Methanol-to-Olefin Conversion over H-ZSM-5 and H-SAPO-34. *Chem. - Eur. J.* **2008**, *14*, 11320−11327.
(34) Mores, D.; Kornatowski, J.; Olsbye, U.; Weckhuysen, B. M. Coke Formation during the Methanol-to-Olefin Conversion: In Situ Microspectroscopy on Individual H-ZSM-5 Crystals with Different Brønsted Acidity. *Chem. - Eur. J.* **2011**, *17*, 2874−2884.
(35) Qian, Q.; Ruiz-Martínez, J.; Mokhtar, M.; Asiri, A. M.; Al-Thabaiti, S. A.; Basahel, S. N.; Weckhuysen, B. M. Single-catalyst particle spectroscopy of alcohol-to-olefins conversions: Comparison between SAPO-34 and SSZ-13. *Catal. Today* **2014**, *226*, 14−24.
(36) Dai, W.; Wu, G.; Li, L.; Guan, N.; Hunger, M. Mechanisms of the Deactivation of SAPO-34 Materials with Different Crystal Sizes Applied as MTO Catalysts. *ACS Catal.* **2013**, *3*, 588−596.
(37) Hereijgers, B. P. C.; Bleken, F.; Nilsen, M. H.; Svelle, S.; Lillerud, K.-P.; Bjørgen, M.; Weckhuysen, B. M.; Olsbye, U. Product shape selectivity dominates the Methanol-to-Olefins (MTO) reaction over H-SAPO-34 catalysts. *J. Catal.* **2009**, *264*, 77−87.
(38) Chang, C. D.; Silvestri, A. J. The Conversion of Methanol and Other O-Compounds to Hydrocarbons over Zeolite Catalysts. *J. Catal.* **1977**, *47*, 249−259.
(39) Teketel, S.; Olsbye, U.; Lillerud, K.-P.; Beato, P.; Svelle, S. Selectivity control through fundamental mechanistic insight in the conversion of methanol to hydrocarbons over zeolites. *Microporous Mesoporous Mater.* **2010**, *136*, 33−41.
(40) Olsbye, U.; Svelle, S.; Bjørgen, M.; Beato, P.; Janssens, T. V. W.; Joensen, F.; Bordiga, S.; Lillerud, K.-P. Conversion of Methanol to Hydrocarbons: How Zeolite Cavity and Pore Size Controls Product Selectivity. *Angew. Chem., Int. Ed.* **2012**, *51*, 5810−5831.
(41) Khare, R.; Millar, D.; Bhan, A. A mechanistic basis for the effects of crystallite size on light olefin selectivity in methanol-to-hydrocarbons conversion on MFI. *J. Catal.* **2015**, *321*, 23−31.
(42) Khare, R.; Bhan, A. Mechanistic studies of methanol-to-hydrocarbons conversion on diffusion-free MFI samples. *J. Catal.* **2015**, *329*, 218−228.
(43) Khare, R.; Liu, Z.; Han, Y.; Bhan, A. A mechanistic basis for the effect of aluminum content on ethene selectivity in methanol-to-hydrocarbons conversion on HZSM-5. *J. Catal.* **2017**, *348*, 300−305.
(44) Arora, S. S.; Bhan, A. The critical role of methanol pressure in controlling its transfer dehydrogenation and the corresponding effect on propylene-to-ethylene ratio during methanol-to-hydrocarbons catalysis on H-ZSM-5. *J. Catal.* **2017**, *356*, 300−306.
(45) Ilias, S.; Khare, R.; Malek, A.; Bhan, A. A descriptor for the relative propagation of the aromatic- and olefin-based cycles in methanol-to-hydrocarbons conversion on H-ZSM-5. *J. Catal.* **2013**, *303*, 135−140.
(46) Hwang, A.; Prieto-Centurion, D.; Bhan, A. Isotopic tracer studies of methanol-to-olefins conversion over HSAPO-34: The role of the olefins-based catalytic cycle. *J. Catal.* **2016**, *337*, 52−56.
(47) Ilias, S.; Bhan, A. Tuning the selectivity of methanol-to-hydrocarbons conversion on H-ZSM-5 by co-processing olefin or aromatic compounds. *J. Catal.* **2012**, *290*, 186−192.
(48) Sun, X.; Müller, S.; Shi, H.; Haller, G. L.; Sanchez-Sanchez, M.; van Veen, A. C.; Lercher, J. A. On the impact of co-feeding aromatics and olefins for the methanol-to-olefins reaction on HZSM-5. *J. Catal.* **2014**, *314*, 21−31.
(49) Khare, R.; Arora, S. S.; Bhan, A. Implications of Cofeeding Acetaldehyde on Ethene Selectivity in Methanol-to-Hydrocarbons Conversion on MFI and Its Mechanistic Interpretation. *ACS Catal.* **2016**, *6*, 2314−2331.
(50) Lok, B. M.; Messina, C. A.; Patton, R. L.; Gajek, R. T.; Cannan, T. R.; Flanigen, E. M. Silicoaluminophosphate Molecular Sieves: Another New Class of Microporous Crystalline Inorganic Solids. *J. Am. Chem. Soc.* **1984**, *106*, 6092−6093.
(51) Hwang, A.; Kumar, M.; Rimer, J. D.; Bhan, A. Implications of methanol disproportionation on catalyst lifetime for methanol-to-olefins conversion by HSSZ-13. *J. Catal.* **2017**, *346*, 154−160.
(52) Zones, S. I. Zeolite SSZ-13 and its method of preparation. U.S. Patent 4,544,538 A, 1983.
(53) Teketel, S.; Svelle, S.; Lillerud, K.-P.; Olsbye, U. Shape-Selective Conversion of Methanol to Hydrocarbons Over 10-Ring Unidirectional-Channel Acidic H-ZSM-22. *ChemCatChem* **2009**, *1*, 78−81.
(54) An alternative hypothesis consistent with the two trends in Figure 1 considers transfer dehydrogenation of species derived from methyl-substituted benzenes as the limiting step in cascades for chain carrier termination. Hydrogen acceptors in methanol-to-hydrocarbons catalysis on solid acids include methanol (vide infra), giving methane and water as the hydrogen-rich coproducts, and olefins, giving $C_{\geq 2}$ alkanes as the hydrogen-rich coproducts. $P_{MeOH,0}$ and SV act in the same direction on the average concentration of methanol but in divergent directions on the average concentration of olefins. If transfer dehydrogenation is the limiting step in chain carrier termination, then the two trends in Figure 1 stipulate that transfer dehydrogenation occurs predominantly with methanol as the hydrogen acceptor (to form CH_4 and H_2O). This seems unlikely because the selectivity for $C_{\geq 2}$ alkanes is always higher than the selectivity for methane, except at very early times on stream when termination is negligible (vide infra), regardless of $P_{MeOH,0}$ and SV.
(55) Schulz, H. "Coking" of zeolites during methanol conversion: Basic reactions of the MTO-, MTP- and MTG processes. *Catal. Today* **2010**, *154*, 183−194.
(56) Wu, E. L.; Kühl, G. H.; Whyte, T. E., Jr.; Venuto, P. B. In *Molecular Sieve Zeolites-I*; Flanigen, E. M., Sand, L. B., Eds.; Advances in Chemistry, Vol. *101*; American Chemical Society, 1971; pp 490−501.
(57) Haag, W. O.; Lago, R. M.; Rodewald, P. G. Aromatics, light olefins and gasoline from methanol: Mechanistic pathways with ZSM-5 zeolite catalyst. *J. Mol. Catal.* **1982**, *17*, 161−169.
(58) Kubelková, L.; Nováková, J.; Jíru, P. Reaction of small amounts of methanol on HZSM-5, HY and modified Y zeolites. *Stud. Surf. Sci. Catal.* **1984**, *18*, 217−224.
(59) Hutchings, G. J.; Gottschalk, F.; Hall, M. V. M.; Hunter, R. Hydrocarbon formation from methylating agents over the zeolite catalyst ZSM-5. Comments on the mechanism of carbon−carbon bond and methane formation. *J. Chem. Soc., Faraday Trans. 1* **1987**, *83*, 571−583.
(60) Hutchings, G. J.; Gottschalk, F.; Hunter, R. Comments on "Kinetic Model for Methanol Conversion to Olefins" with Respect to Methane Formation at Low Conversion. *Ind. Eng. Chem. Res.* **1987**, *26*, 635−637.
(61) Dewaele, O.; Geers, V. L.; Froment, G. F.; Marin, G. B. The conversion of methanol to olefins: A transient kinetic study. *Chem. Eng. Sci.* **1999**, *54*, 4385−4395.
(62) Wei, Z.; Chen, Y.-Y.; Li, J.; Wang, P.; Jing, B.; He, Y.; Dong, M.; Jiao, H.; Qin, Z.; Wang, J.; Fan, W. Methane formation mechanism in the initial methanol-to-olefins process catalyzed by SAPO-34. *Catal. Sci. Technol.* **2016**, *6*, 5526−5533.

DOI: 10.1021/acs.accounts.9b00204
Acc. Chem. Res. 2019, 52, 2647−2656

(63) Walker, J. F. *Formaldehyde*, 3rd ed.; Reinhold Publishing, 1964.
(64) Liu, Y.; Kirchberger, F. M.; Müller, S.; Eder, M.; Tonigold, M.; Sanchez-Sanchez, M.; Lercher, J. A. Critical role of formaldehyde during methanol conversion to hydrocarbons. *Nat. Commun.* **2019**, *10*, 1462.
(65) Arundale, E.; Mikeska, L. A. The Olefin−Aldehyde Condensation. The Prins Reaction. *Chem. Rev.* **1952**, *51*, 505−555.
(66) Dumitriu, E.; Trong On, D.; Kaliaguine, S. Isoprene by Prins Condensation over Acidic Molecular Sieves. *J. Catal.* **1997**, *170*, 150−160.
(67) Climent, M. J.; Corma, A.; García, H.; Primo, J. Zeolites in organic reactions: Condensation of formaldehyde with benzene in the presence of HY zeolites. *Appl. Catal.* **1989**, *51*, 113−125.
(68) Li, Y.; Zhang, M.; Wang, D.; Wei, F.; Wang, Y. Differences in the methanol-to-olefins reaction catalyzed by SAPO-34 with dimethyl ether as reactant. *J. Catal.* **2014**, *311*, 281−287.
(69) Blaszkowski, S. R.; van Santen, R. A. The Mechanism of Dimethyl Ether Formation from Methanol Catalyzed by Zeolitic Protons. *J. Am. Chem. Soc.* **1996**, *118*, 5152−5153.
(70) Jones, A. J.; Iglesia, E. Kinetic, Spectroscopic, and Theoretical Assessment of Associative and Dissociative Methanol Dehydration Routes in Zeolites. *Angew. Chem., Int. Ed.* **2014**, *53*, 12177−12181.
(71) Sun, X.; Müller, S.; Liu, Y.; Shi, H.; Haller, G. L.; Sanchez-Sanchez, M.; van Veen, A. C.; Lercher, J. A. On reaction pathways in the conversion of methanol to hydrocarbons on HZSM-5. *J. Catal.* **2014**, *317*, 185−197.
(72) Müller, S.; Liu, Y.; Vishnuvarthan, M.; Sun, X.; van Veen, A. C.; Haller, G. L.; Sanchez-Sanchez, M.; Lercher, J. A. Coke formation and deactivation pathways on H-ZSM-5 in the conversion of methanol to olefins. *J. Catal.* **2015**, *325*, 48−59.
(73) Müller, S.; Liu, Y.; Kirchberger, F. M.; Tonigold, M.; Sanchez-Sanchez, M.; Lercher, J. A. Hydrogen Transfer Pathways during Zeolite Catalyzed Methanol Conversion to Hydrocarbons. *J. Am. Chem. Soc.* **2016**, *138*, 15994−16003.
(74) Martinez-Espin, J. S.; Mortén, M.; Janssens, T. V. W.; Svelle, S.; Beato, P.; Olsbye, U. New insights into catalyst deactivation and product distribution of zeolites in the methanol-to-hydrocarbons (MTH) reaction with methanol and dimethyl ether feeds. *Catal. Sci. Technol.* **2017**, *7*, 2700−2716.
(75) Martinez-Espin, J. S.; De Wispelaere, K.; Westgård Erichsen, M.; Svelle, S.; Janssens, T. V. W.; Van Speybroeck, V.; Beato, P.; Olsbye, U. Benzene co-reaction with methanol and dimethyl ether over zeolite and zeotype catalysts: Evidence of parallel reaction paths to toluene and diphenylmethane. *J. Catal.* **2017**, *349*, 136−148.
(76) Martinez-Espin, J. S.; De Wispelaere, K.; Janssens, T. V. W.; Svelle, S.; Lillerud, K. P.; Beato, P.; Van Speybroeck, V.; Olsbye, U. Hydrogen Transfer versus Methylation: On the Genesis of Aromatics Formation in the Methanol-to-Hydrocarbons Reaction over H-ZSM-5. *ACS Catal.* **2017**, *7*, 5773−5780.
(77) "Reaction progress" is the cumulative number of moles of methanol converted to hydrocarbon products per mole of H^+ in the catalyst bed, i.e., $\int_0^t \mathrm{SV}\cdot X(t')\,\mathrm{d}t'$, where t is time-on-stream, SV is space velocity, and X is conversion of methanol to hydrocarbons ($X(t) = \sum_{m,n} m \cdot F_{\mathrm{C}_m\mathrm{H}_n}(t)/F_{\mathrm{MeOH},0}$).
(78) Levin, D.; Vartuli, J. C. Molecular Sieve Compositions, Catalysts Thereof, Their Making and Use in Conversion Processes. U.S. Patent 6,995,111, 2003.
(79) Nieskens, D. L. S.; Ferrari, D.; Liu, Y.; de Putter, S. A. Effect of Oxygenate Impurities on the Conversion of Alcohols to Olefins. *Ind. Eng. Chem. Res.* **2014**, *53*, 10892−10898.
(80) Hwang, A.; Bhan, A. Bifunctional Strategy Coupling Y_2O_3-Catalyzed Alkanal Decomposition with Methanol-to-Olefins Catalysis for Enhanced Lifetime. *ACS Catal.* **2017**, *7*, 4417−4422.
(81) Weisz, P. Polyfunctional Heterogeneous Catalysis. *Adv. Catal.* **1962**, *13*, 137−190.
(82) Rosynek, M. P.; Magnuson, D. T. Infrared study of carbon dioxide adsorption on lanthanum sesquioxide and trihydroxide. *J. Catal.* **1977**, *48*, 417−421.
(83) Rosynek, M. P. Catalytic Properties of Rare Earth Oxides. *Catal. Rev.: Sci. Eng.* **1977**, *16*, 111−154.
(84) Rosynek, M. P.; Koprowski, R. J.; Dellisante, G. N. The Nature of Catalytic Sites on Lanthanum and Neodymium Oxides for Dehydration/Dehydrogenation of Ethanol. *J. Catal.* **1990**, *122*, 80−94.
(85) Hattori, H. Heterogeneous Basic Catalysis. *Chem. Rev.* **1995**, *95*, 537−558.
(86) Hussein, G. A. M.; Gates, B. C. Surface and Catalytic Properties of Yttrium Oxide: Evidence from Infrared Spectroscopy. *J. Catal.* **1998**, *176*, 395−404.
(87) Sato, S.; Takahashi, R.; Kobune, M.; Gotoh, H. Basic properties of rare earth oxides. *Appl. Catal., A* **2009**, *356*, 57−63.
(88) Hwang, A. Mechanisms of Chain Carrier Propagation and Termination in Methanol-to-Olefins Catalysis on Small Pore Zeotypes and Zeolites. Ph.D. Thesis, University of Minnesota, 2018.
(89) Cannizzaro, S. Ueber den der Benzoësäure entsprechenden Alkohol. *Justus Liebigs Ann. Chem. Pharm.* **1853**, *88*, 129−130.
(90) Peng, X. D.; Barteau, M. A. Adsorption of formaldehyde on model magnesia surfaces: Evidence for the Cannizzaro reaction. *Langmuir* **1989**, *5*, 1051−1056.
(91) Zhan, B.-Z.; Iglesia, E. RuO_2 Clusters within LTA Zeolite Cages: Consequences of Encapsulation on Catalytic Reactivity and Selectivity. *Angew. Chem., Int. Ed.* **2007**, *46*, 3697−3700.
(92) Otto, T.; Zones, S. I.; Hong, Y.; Iglesia, E. Synthesis of highly dispersed cobalt oxide clusters encapsulated within LTA zeolites. *J. Catal.* **2017**, *356*, 173−185.
(93) Otto, T.; Zones, S. I.; Iglesia, E. Synthetic strategies for the encapsulation of nanoparticles of Ni, Co, and Fe oxides within crystalline microporous aluminosilicates. *Microporous Mesoporous Mater.* **2018**, *270*, 10−23.
(94) We did not measure precisely the turnover number for the reaction with 30 bar H_2 because the reaction exhibits little deactivation after 130 h (ca. −6% change in conversion). A "relative change in turnover number" of 70 is a very conservative estimate, and the gray upward-pointing arrow attendant to this data point in Figure 6 is meant to convey the underestimation. The black dashed line in Figure 6 is a guide for the eye, while the gray dashed line represents an extrapolation for values of "relative change in turnover number" at hydrogen pressures greater than 15 bar.
(95) Arora, S. S.; Nieskens, D. L. S.; Malek, A.; Bhan, A. Lifetime improvement in methanol-to-olefins catalysis over chabazite materials by high pressure H_2 co-feeds. *Nat. Catal.* **2018**, *1*, 666−672.
(96) Senger, S.; Radom, L. Zeolites as Transition-Metal-Free Hydrogenation Catalysts: A Theoretical Mechanistic Study. *J. Am. Chem. Soc.* **2000**, *122*, 2613−2620.
(97) Gounder, R.; Iglesia, E. Catalytic hydrogenation of alkenes on acidic zeolites: Mechanistic connections to monomolecular alkane dehydrogenation reactions. *J. Catal.* **2011**, *277*, 36−45.
(98) Arora, S. S.; Shi, Z.; Bhan, A. A mechanistic basis for effects of high-pressure H_2 co-feeds on methanol-to-hydrocarbons catalysis over zeolites. *ACS Catal.* **2019**, *9*, 6407−6414.
(99) Jong, S.-J.; Pradhan, A. R.; Wu, J.-F.; Tsai, T.-C.; Liu, S.-B. On the regeneration of coked H-ZSM-5 catalysts. *J. Catal.* **1998**, *174*, 210−218.
(100) Scherzer, J.; Gruia, A. J. *Hydrocracking Science and Technology*, 1st ed.; CRC Press, 1996.
(101) Bercaw, J. E.; Grubbs, R. H.; Hazari, N.; Labinger, J. A.; Li, X. Enhanced selectivity in the conversion of methanol to 2,2,3-trimethylbutane (triptane) over zinc iodide by added phosphorous or hypophosphorous acid. *Chem. Commun.* **2007**, 2974−2976.
(102) Mayr, H.; Lang, G.; Ofial, A. R. Reactions of Carbocations with Unsaturated Hydrocarbons: Electrophilic Alkylation or Hydride Abstraction? *J. Am. Chem. Soc.* **2002**, *124*, 4076−4083.
(103) Gounder, R.; Iglesia, E. Catalytic Alkylation Routes via Carbonium-Ion-Like Transition States on Acidic Zeolites. *ChemCatChem* **2011**, *3*, 1134−1138.

DOI: 10.1021/acs.accounts.9b00204
Acc. Chem. Res. 2019, 52, 2647−2656